

RadarFuseNet: Complex-Valued Attention-Based Fusion of IQ Time- and Frequency-Domain Radar Features for Classification Tasks

Stefan Hägele, Adam Misik and Eckehard Steinbach

Technical University of Munich

School of Computation, Information and Technology

Chair of Media Technology

Munich Institute of Robotics and Machine Intelligence

{stefan.haegele, adam.misik, eckehard.steinbach}@tum.de

Abstract—Millimeter-wave (mmWave) radar has emerged as a compact and powerful sensing modality for advanced perception tasks that leverage machine learning techniques. It is particularly effective in scenarios where vision-based sensors fail to capture reliable information, such as detecting occluded objects or distinguishing between different surface materials in indoor environments. Due to the non-linear characteristics of mmWave radar signals, deep learning-based methods are well suited for extracting relevant information from in-phase and quadrature (IQ) data. However, the current state of the art in IQ signal-based occluded-object and material classification still offers substantial potential for further improvement. In this paper, we propose a bidirectional cross-attention fusion network that combines IQ-signal and FFT-transformed radar features obtained by distinct complex-valued convolutional neural networks (CNNs). The proposed method achieves improved performance and robustness compared to standalone complex-valued CNNs. We achieve a near-perfect material classification accuracy of 99.92% on samples collected at same sensor-to-surface distances used during training, and an improved accuracy of 67.38% on samples measured at previously unseen distances, demonstrating improved generalization ability across varying measurement conditions. Furthermore, the accuracy for occluded object classification improves from 91.99% using standalone complex-valued CNNs to 94.20% using our proposed approach.

Index Terms—mmWave radar, classification, feature fusion, deep learning, signal processing

I. INTRODUCTION

Millimeter-wave (mmWave) radar is an effective sensing modality for various perception tasks, particularly in scenarios where camera- or LiDAR-based sensors are undesirable or impractical. This advantage is further supported by the widespread availability, low cost, and adequate sensing resolution, particularly in challenging environments such as rain, fog, smoke, or under occlusions [1]–[3]. Furthermore, the distinctive reflective signatures of mmWave radar enable the recognition and classification of various surface materials [4]. Recent research in radar-based deep learning has

The authors acknowledge the financial support by the Federal Ministry of Research, Technology and Space of Germany in the programme of “Souverän. Digital. Vernetzt.”. Joint project 6G-life, project identification number: 16KISK002

primarily focused on processing radar signals as image-like representations, such as range–angle or range–Doppler maps, as well as on sparse point clouds obtained using a CFAR algorithm [5], [6]. Since these signal-to-image or signal-to-point-cloud transformations discard certain information, such as phase, our goal is to focus instead on directly utilizing the complex-valued in-phase and quadrature (IQ) signal of the mmWave radar. Previous work in this field has investigated the classification of various objects (occluded by light materials and non-occluded), as well as different surface materials, with the goal of enhancing indoor perception with mmWave radar through direct processing of complex-valued IQ signals [4], [7]. Both tasks still exhibit room for improvement, particularly surface material classification, which tends to perform poorly at unknown or untrained sensing distances to the target surface. To enhance feature representation, we propose RadarFuseNet, an attention-based fusion mechanism for raw IQ and FFT-transformed complex-valued radar signals. For this purpose, we employ two complex-valued CNNs to extract separate features from the IQ signal and its FFT-transformed counterpart, which are subsequently fused using a cross-attention mechanism. This enables leveraging two complementary feature spaces to extract and fuse richer feature representations. Although the theoretical information content is identical in both signal representations, our goal is to optimize feature availability, thereby providing the final model with a more effective learning foundation. Our main contributions are summarized as follows:

- Design of an architecture integrating two complex-valued CNNs with a bidirectional cross-attention fusion mechanism for complex-valued radar signals.
- Adaptation of complex-valued feature representations for compatibility with real-valued cross-attention processing.
- Demonstration of improved generalization and robustness under varying measurement conditions.

The remainder of this paper is organized as follows. Section II reviews related work in recent mmWave radar research and radar-based deep learning. Section III presents the proposed

methodology, including signal pre-processing and model architecture. Section IV reports the experimental results and evaluation, while Section V concludes the paper and outlines directions for future research.

II. RELATED WORK

Millimeter wave (mmWave) radar has gained significant momentum in recent years, with extensive research being conducted in diverse fields such as autonomous driving, object tracking, gesture recognition and human activity understanding. This development is mainly driven by the increased availability of affordable, high-resolution radar hardware. Additionally, radar's robustness under adverse environmental conditions makes it a valuable complement to existing perception approaches, particularly in the automotive domain. There, most deep learning-based approaches employ fusion strategies that combines RGB-D images with radar/LiDAR data to enhance robustness and improve depth estimation. In addition to approaches utilizing convolutional neural networks (CNNs) or any type of neural network (NN) for feature extraction, more recent methods incorporate attention-based models to further enhance perception accuracy and fusion quality [5], [6], [8]–[10]. However, the input data type used in these fusion approaches is typically radar heatmap images (range–angle or range–Doppler) or point clouds, rather than directly a complex-valued analog-to-digital converted (ADC) radar signal. The ADC signal retains both amplitude and phase information, avoiding the loss that occurs when converting it into an image representation. A main reason for this limitation, especially in the automotive domain, is the scarcity of publicly available datasets containing such data. A similar picture arises when looking at publicly available datasets for gesture recognition and human activity understanding [11], [12]. Similarly, alongside more traditional deep learning approaches that employ micro-Doppler signatures and neural networks, recent research has demonstrated the advantages of attention-based deep learning models in enhancing robustness and accuracy [13]–[15]. In most applications, feature fusion typically involves combining two fundamentally different sensor modalities to enhance overall perception performance, such as camera and radar or LiDAR. However, in the context of mmWave radar, limited research has investigated the fusion of different representations of the same signal, aiming not to increase the informational content but to improve the extractability of features. Although recent research has investigated GNSS signals using time–frequency domain fusion, mmWave radar was not subject of evaluation in these studies [16]. In our work, we integrate an adapted version of this approach with complex-valued CNNs for feature extraction of radar features [17]. For performance evaluation, two of our previously recorded datasets are used. These datasets, introduced in [4] and [7], are used for surface material classification and occluded object classification, respectively. [4] introduced a complex-valued CNN for processing complex-valued radar inputs, which is adopted as the feature extractor in our proposed model. Both datasets were recorded using a high-resolution mmWave

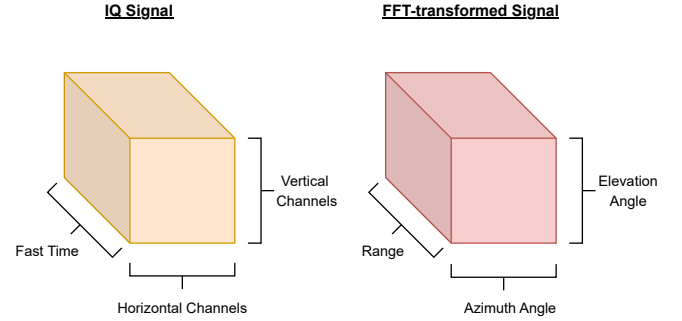


Fig. 1: Dimensions of the raw IQ signal (left) and its FFT-transformed counterpart (right).

FMCW MIMO imaging radar sensor from Vayyar with an L-shaped 20×20 antenna configuration. The sensor provides a complex-valued intermediate frequency (IF) IQ output and operates within an RF frequency range of 62–69 GHz [18]. The two different signal types used for classification serve to evaluate the overall robustness and applicability for different tasks of the proposed approach. The data can be found at <https://github.com/haegels/radar-IQ-datasets>.

III. METHODOLOGY

A. Signal Pre-processing

With its 20×20 L-shaped antenna configuration, the radar sensor provides a 400-channel sample s per measurement, with each channel sampled at 100 time points. The dimensions of s are shown in Eq. 1. Each sample contains a single FMCW chirp, as Doppler information is unnecessary due to the static nature of the targets. Overall, the signal can be represented as a 3D data cube, illustrated in Fig. 1, along with its respective dimensional interpretation.

$$s \in \mathbb{C}^{20 \times 20 \times 100} \quad (1)$$

To fuse time- and frequency domain data, spectral and raw IQ versions of the signal are required. A 3D fast Fourier transform (FFT) is applied to the signal cube s and provides the range-, azimuth- and elevation spectrum S of the signal. This process is formalized in Eq. 2, where n denotes the fast-time dimension and x and y represent the spatial dimensions:

$$S(l, m, k) = \sum_{x=0}^{X-1} \sum_{y=0}^{Y-1} \sum_{n=0}^{N-1} s(x, y, n) e^{-j2\pi(\frac{lx}{X} + \frac{my}{Y} + \frac{kn}{N})} \quad (2)$$

l , m , and k are their corresponding transformed counterparts, representing the range and angle bins in both directions of equal size as s . To meet the input requirements of the complex-valued CNN, both signals s and S are reshaped into 2D representations x and X by flattening along the channel dimension, such that

$$x, X \in \mathbb{C}^{(20 \cdot 20) \times 100}. \quad (3)$$

This results in two signal types ready to be used as CNN inputs, \mathbf{x} representing the time-domain IQ signal and \mathbf{X} its FFT-transformed counterpart, which includes the azimuth and elevation angle profiles as well as the range profile in the complex domain.

B. Model Architecture

Two distinct complex-valued CNNs are used to extract features in RadarFuseNet. One processes the raw IQ signal \mathbf{x} , while the other processes its FFT-transformed version \mathbf{X} . All operations in these feature-extracting CNNs are performed in the complex domain, including convolutions, pooling, batch normalization, and ReLU activation functions [17]. The complex-valued convolution and complex-valued ReLU function are defined in Eq. 4 and Eq. 6, respectively. Furthermore, batch normalization (Eq. 5) and pooling are applied in a naive manner, performed separately on the real and imaginary components. The complex-valued structure is advantageous, as it enables direct processing and feature extraction from the complete signal without separating its real and imaginary components. This allows features to be derived from the intact signal phasor rather than from a split and concatenated representation. For kernels $k = a + jb \in \mathbb{C}$ and input $x = c + jd \in \mathbb{C}$, the convolution emerges as

$$k \cdot x = c \cdot a - d \cdot b + j(c \cdot b + d \cdot a), \quad (4)$$

and for batch normalization (BN) of $z \in \mathbb{C}$

$$cBN(z) = BN(Re\{z\}) + jBN(Im\{z\}). \quad (5)$$

The complex-valued ReLU activation function is defined as

$$cReLU(z) \begin{cases} z, & \text{if } Re\{z\}, Im\{z\} \geq 0 \\ 0, & \text{else.} \end{cases} \quad (6)$$

The overall architecture is shown in Fig. 2. Both CNN branches share the same structure, adopted from SMCNet for complex-valued radar signals [4]. It is depicted in Fig. 3, realized with three complex layers and complex average pooling. Before feature fusion, the complex-valued features \mathbf{f} (IQ features) and \mathbf{F} (FFT features) are converted to real-valued versions $\tilde{\mathbf{f}}$ and $\tilde{\mathbf{F}}$. This is done by concatenating their real and imaginary components, as the cross-attention module requires real-valued input. This procedure is applied to both feature vectors in the same manner to ensure positional coherence. Due to its design, the cross-attention mechanism can still capture relationships between features, even after the signal is transformed into the real domain. IQ and FFT representations are fused through a bidirectional cross-attention mechanism, wherein $\tilde{\mathbf{f}}$ attends to $\tilde{\mathbf{F}}$ and vice versa. This encourages richer cross-domain feature alignment. The resulting representations are then concatenated to form a unified bidirectional cross-attention output. The formula for computing the cross-attention is defined in Eq. 7.

$$\text{Attn}(Q, K, V) = \text{softmax} \left(\frac{QK^\top}{\sqrt{d_k}} \right) V \quad (7)$$

TABLE I: Radar configuration parameters for both evaluation datasets.

Parameters	Material Samples [4]	Occluded Objects [7]
Center Frequency f_c	65.5GHz	64GHz
Bandwidth B	5GHz	4GHz
EIRP (dBm)	-5dBm	-5dBm
Number Tx/Rx Antennas	20/20	20/20
Sample Points (fast time)	100	100

Q , K , and V represent the queries, keys, and values, respectively, while d_k is the dimensionality of the key vectors. For feature inputs $\tilde{\mathbf{f}}$ and $\tilde{\mathbf{F}}$, the following operations are performed:

$$A_1 = \text{Attn}(\tilde{\mathbf{f}}, \tilde{\mathbf{F}}, \tilde{\mathbf{F}}) \quad (8)$$

$$A_2 = \text{Attn}(\tilde{\mathbf{F}}, \tilde{\mathbf{f}}, \tilde{\mathbf{f}}) \quad (9)$$

$$A = \text{concat}(A_1, A_2) \quad (10)$$

A denotes the output of a single attention head and the concatenation of A_1 and A_2 . We employ multi-head cross-attention with an embedding dimension of 256 and 16 heads, applying a 16-way concatenation of the projections defined in Eq. 10. As the task is classification, a single fully connected layer followed by a cross-entropy loss function is applied to obtain the final prediction. The cross-entropy loss is defined as

$$H(\hat{\xi}, \xi) = - \sum_{j=1}^C \xi_j \log(\hat{\xi}_j), \quad (11)$$

where $\hat{\xi}$ and ξ are the predicted- and target distributions, respectively. C represents the number of object classes.

IV. RESULTS

We evaluate the performance gain achieved by fusing IQ and FFT representations. The results are compared against the single-branch baseline model shown in Fig. 3, which uses only the FFT representation without feature fusion. This serves as the baseline signal format for comparison, allowing a clear assessment of the benefit introduced by the fusion strategy. In general, the FFT representation provides richer discriminative features than the raw IQ domain, as demonstrated in [4]. This makes it suitable as a baseline. The datasets for evaluation contain:

- Five surface materials in indoor environments, with three sensor-to-surface distances for training and two additional distances only used for testing (concrete, drywall, glass, metal, wood).
- Ten occluded objects placed inside a cardboard box (ball, cable, calculator, deodorant, hammer, mug, plastic cup, screwdriver, tape, bottle).

The data collection setups are illustrated in Fig. 4 and the configuration of the Vayyar radar sensor used for data collection is summarized in Table I. A conventional 80/20 training and testing split was used, with additional test samples from untrained distances for the material dataset. These are additional test samples evaluated separately, not included in

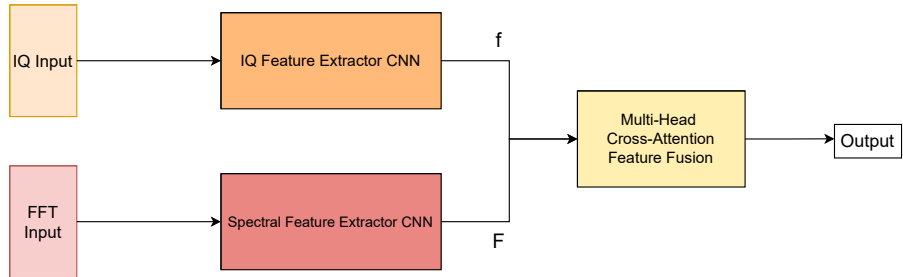


Fig. 2: Model architecture including two complex-valued CNNs for IQ- (f) and FFT (F) feature extraction, and a multi-head cross-attention mechanism to fuse the extracted features.

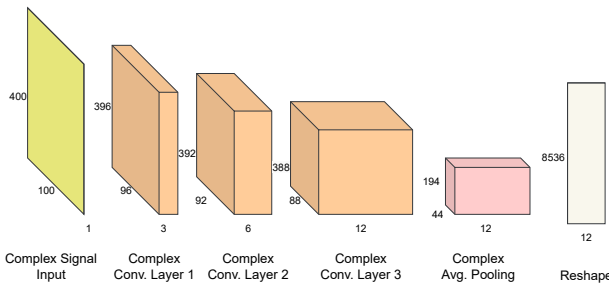


Fig. 3: Design of the single-branch complex-valued CNN feature extractor.



Fig. 4: Setups for surface material data collection (left) and occluded object data collection (right) [4], [7].

the conventional 20% test set for material classification. The occluded object dataset contains approximately 500 samples, whereas the surface material dataset comprises around 1000 samples. A batch size of 16 was used for training, with the Adam optimizer and a learning rate of 0.001 over 15 epochs. Tables II and III present the results of the single-branch CNN classifier baseline and the proposed RadarFuseNet model.

TABLE II: Overall accuracy of radar models for occluded object classification.

Model	Occluded Objects Accuracy
Single-branch CNN RadarFuseNet	91.99 % 94.20 %

TABLE III: Overall accuracy of radar models for material classification.

Model	Material Accuracy (known distance)	Material Accuracy (unknown distance)
Single-branch CNN RadarFuseNet	99.95 % 99.92 %	55.94 % 67.38 %

In general, the occluded object dataset is more diverse than the surface material dataset, as it includes a larger number of classes. A significant improvement in overall accuracy is observed when applying the proposed fusion model to the occluded object dataset, indicating better overall generalization compared to the baseline. However, the occluded object samples were collected at a fixed sensor-to-object distance, whereas the surface material samples were acquired at three different sensor-to-surface distances. The performance on trained (known) distances is already very high for both approaches, with no substantial differences observed. However, when evaluated on unseen sensor-to-surface distances not included in the training process, a significant improvement in accuracy is observed with our proposed RadarFuseNet. This demonstrates an enhanced overall generalization capability. The improvement is evidenced by higher accuracy on occluded objects and increased robustness to varying measurement distances in the material dataset. However, both results still leave room for improvement. As both datasets used for evaluation are relatively small, there is an increased risk of overfitting and reduced generalization performance. Collecting more diverse and complex data would help further assess the extent of overall improvement and reveal potential limitations of the proposed approach. This will be subject for potential future work.

V. CONCLUSION AND FUTURE WORK

In this paper, we introduced RadarFuseNet, a model that employs bidirectional cross-attention to fuse raw mmWave radar IQ features with their FFT-transformed representations. Both feature types are extracted using complex-valued CNNs specifically designed to process complex-valued input data, rather than radar images. This fusion approach enhances feature availability and improves their learnability within the model. An overall increase in accuracy was observed across

both evaluated datasets, indicating improved robustness and stronger generalization capability compared to a single-branch complex-valued CNN baseline. Certain limitations remain, as the employed IQ radar datasets are relatively small in size. A key direction for future work is to develop an enhanced version of the model capable of handling larger and more diverse datasets, alongside the collection of such data. However, for current application scenarios and available IQ radar datasets, RadarFuseNet proves to be a strong model, offering high robustness and accuracy.

REFERENCES

- [1] S. Zang, M. Ding, D. Smith, P. Tyler, T. Rakotoarivelo and M. A. Kaafar, "The Impact of Adverse Weather Conditions on Autonomous Vehicles: How Rain, Snow, Fog, and Hail Affect the Performance of a Self-Driving Car," in IEEE Vehicular Technology Magazine, vol. 14, no. 2, pp. 103-111, June 2019, doi: 10.1109/MVT.2019.2892497.
- [2] H. Kulhandjian, A. Davis, L. Leong, M. Bendot and M. Kulhandjian, "AI-based Human Detection and Localization in Heavy Smoke using Radar and IR Camera," 2023 IEEE Radar Conference (RadarConf23), San Antonio, TX, USA, 2023, pp. 1-6, doi: 10.1109/RadarConf2351548.2023.10149735.
- [3] M. A. Maisto, M. Masoodi, R. Pierri and R. Solimene, "Sensor Arrangement in Through-the Wall Radar Imaging," in IEEE Open Journal of Antennas and Propagation, vol. 3, pp. 333-341, 2022, doi: 10.1109/OJAP.2022.3159279.
- [4] S. Hägele, F. Seguel, D. Salihu, A. Misik and E. Steinbach, "SM-CNet: Supervised Surface Material Classification Using mmWave Radar IQ Signals and Complex-valued CNNs," ICASSP 2025 - 2025 IEEE International Conference on Acoustics, Speech and Signal Processing (ICASSP), Hyderabad, India, 2025, pp. 1-5, doi: 10.1109/ICASSP49660.2025.10890769.
- [5] P. Wolters et al., "Unleashing HyDRA: Hybrid Fusion, Depth Consistency and Radar for Unified 3D Perception," 2025 IEEE International Conference on Robotics and Automation (ICRA), Atlanta, GA, USA, 2025, pp. 7467-7474, doi: 10.1109/ICRA55743.2025.11127412.
- [6] P. Wolters, J. Gilg, T. Teepe and G. Rigoll, "SpaRC-AD: A Baseline for Radar-Camera Fusion in End-to-End Autonomous Driving", arXiv.org, 2025.
- [7] S. Hägele, F. Seguel, S. M. Kahya and E. Steinbach, "Occluded Object Classification With mmWave MIMO Radar IQ Signals Using Dual-Stream Convolutional Neural Networks," in IEEE Transactions on Radar Systems, vol. 3, pp. 789-798, 2025, doi: 10.1109/TRS.2025.3571284.
- [8] Y. Man, L. -Y. Gui and Y. -X. Wang, "BEV-Guided Multi-Modality Fusion for Driving Perception," 2023 IEEE/CVF Conference on Computer Vision and Pattern Recognition (CVPR), Vancouver, BC, Canada, 2023, pp. 21960-21969, doi: 10.1109/CVPR52729.2023.02103.
- [9] L. Fan, J. Wang, Y. Chang, Y. Li, Y. Wang and D. Cao, "4D mmWave Radar for Autonomous Driving Perception: A Comprehensive Survey," in IEEE Transactions on Intelligent Vehicles, vol. 9, no. 4, pp. 4606-4620, April 2024, doi: 10.1109/TIV.2024.3380244.
- [10] S. Yao et al., "Radar-Camera Fusion for Object Detection and Semantic Segmentation in Autonomous Driving: A Comprehensive Review," in IEEE Transactions on Intelligent Vehicles, vol. 9, no. 1, pp. 2094-2128, Jan. 2024, doi: 10.1109/TIV.2023.3307157.
- [11] Y. Li et al., "Towards Domain-Independent and Real-Time Gesture Recognition Using mmWave Signal," in IEEE Transactions on Mobile Computing, vol. 22, no. 12, pp. 7355-7369, Dec. 2023, doi: 10.1109/TMC.2022.3207570.
- [12] Y. Wang, H. Liu, K. Cui, A. Zhou, W. Li and H. Ma, "m-Activity: Accurate and Real-Time Human Activity Recognition Via Millimeter Wave Radar," ICASSP 2021 - 2021 IEEE International Conference on Acoustics, Speech and Signal Processing (ICASSP), Toronto, ON, Canada, 2021, pp. 8298-8302, doi: 10.1109/ICASSP39728.2021.9414686.
- [13] I. Khan and Y. -W. Kwon, "Radar-Based Hand Gesture Recognition With Feature Fusion Using Robust CNN-LSTM and Attention Architecture," in IEEE Access, vol. 13, pp. 69281-69291, 2025, doi: 10.1109/ACCESS.2025.3558293.
- [14] S. Hazra and A. Santra, "Radar Gesture Recognition System in Presence of Interference using Self-Attention Neural Network," 2019 18th IEEE International Conference On Machine Learning And Applications (ICMLA), Boca Raton, FL, USA, 2019, pp. 1409-1414, doi: 10.1109/ICMLA.2019.00230.
- [15] G. Lai, X. Lou and W. Ye, "Radar-Based Human Activity Recognition With 1-D Dense Attention Network," in IEEE Geoscience and Remote Sensing Letters, vol. 19, pp. 1-5, 2022, Art no. 3502505, doi: 10.1109/LGRS.2020.3045176.
- [16] L. Heublein, C. Wielenberg, T. Nowak, T. Feigl, C. Mutschler and F. Ott, "Attention-Based Fusion of IQ and FFT Spectrograms with AoA Features for GNSS Jammer Localization," arXiv preprint arXiv:2507.14167v2, accepted at RadarConf'25, Jul. 2025.
- [17] F. Seguel, D. Salihu, S. Hägele and E. Steinbach, "Complex-valued Deep Learning for WiFi-based Indoor Positioning: Method and performance," European Wireless 2024; 29th European Wireless Conference, Brno, Czech Republic, 2024, pp. 59-65.
- [18] IMAGEVK-74 4D Imaging Radar, Mini-Circuits and Vayyar, https://www.minicircuits.com/WebStore/imagevk_74.html